Front. Chem. Sci. Eng. 2018, 12(3): 564–576
https://doi.org/10.1007/s11705-018-1720-0

REVIEW ARTICLE

Corrosion behavior of metallic alloys in molten chloride salts for thermal energy storage in concentrated solar power plants: A review

Wenjin Ding (✉)[1], Alexander Bonk[1], Thomas Bauer[2]

1 Institute of Engineering Thermodynamics, German Aerospace Center (DLR), 70569 Stuttgart, Germany
2 Institute of Engineering Thermodynamics, German Aerospace Center (DLR), 51147 Cologne, Germany

Abstract Recently, more and more attention is paid on applications of molten chlorides in concentrated solar power (CSP) plants as high-temperature thermal energy storage (TES) and heat transfer fluid (HTF) materials due to their high thermal stability limits and low prices, compared to the commercial TES/HTF materials in CSP-nitrate salt mixtures. A higher TES/HTF operating temperature leads to higher efficiency of thermal to electrical energy conversion of the power block in CSP, however causes additional challenges, particularly increased corrosiveness of metallic alloys used as containers and structural materials. Thus, it is essential to study corrosion behaviors and mechanisms of metallic alloys in molten chlorides at operating temperatures (500–800 °C) for realizing the commercial application of molten chlorides in CSP. The results of studies on hot corrosion of metallic alloys in molten chlorides are reviewed to understand their corrosion behaviors and mechanisms under various conditions (e.g., temperature, atmosphere). Emphasis has also been given on salt purification to reduce corrosive impurities in molten chlorides and development of electrochemical techniques to *in-situ* monitor corrosive impurities in molten chlorides, in order to efficiently control corrosion rates of metallic alloys in molten chlorides to meet the requirements of industrial applications.

Keywords corrosion mechanisms, impurities, metallic corrosion, salt purification, electrochemical techniques

Received January 22, 2018; accepted March 1, 2018

E-mail: wenjin.ding@dlr.de

1 Introduction

Molten chlorides have wide applications in industrial processes, e.g., as electrolytes in high-temperature electrochemical plating and extraction of metals such as Li, Na, Ca and Mg [1–3]. Recently, more and more attention is paid on their promising applications as high-temperature thermal energy storage (TES) and heat transfer fluid (HTF) materials in concentrated solar power (CSP) plants [4,5] due to their good thermophysical properties and low prices. Over the course of the SunShot Initiative, the U.S. Department of Energy has supported the molten chloride salt development for the next generation CSP [4].

CSP technology is emerging as one important technology in the future renewable energy system. It is reported that global installed CSP-capacity has increased nearly fifteen-fold from 2005 to 2015 (up to 4.8 Gigawatts) and grew at an average rate of 50 percent per year from 2010 to 2015 (see Fig. 18 in [6]). In CSP plants as illustrated in Fig. 1, inexpensive storage of the heat from sunlight in TES materials such as molten salts allows them to generate dispatchable power during the absence of sunlight and adds value to such power plants. In commercial CSP plants, a non-eutectic salt mixture of 60 wt-% sodium nitrate and 40 wt-% potassium nitrate, commonly known as solar salt, is typically utilized as the TES material. For instance, the 110-MWe Crescent Dunes tower CSP plant (see Fig. 2) in Nevada, USA, uses ~32000 tons solar salt for 10 h of storage and realizes an annual capacity factor of 52%. Figure 3 shows a molten salt storage tank (container) for this CSP plant, which has huge size, 12.2 m tall and 42.7 m in diameter.

However, as solar salt decomposes at temperatures around 550 °C [7,8], the temperature difference (or heat storage capacity) defined by the hot and cold salt temperature is limited. More importantly, it would be

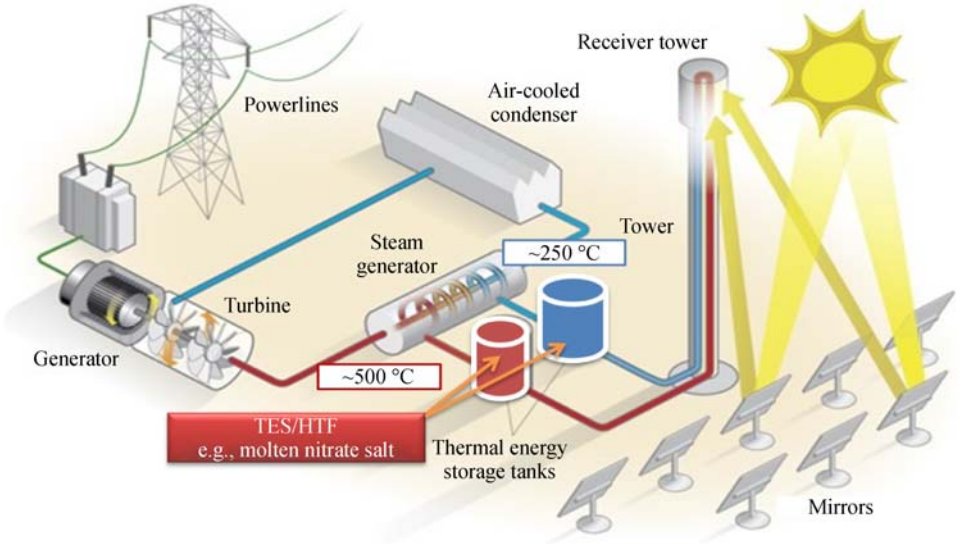

Fig. 1 Concentrated solar power plants with molten salts as TES and HTF materials (source: US Department of Energy)

Fig. 2 110-MWe Crescent Dunes tower CSP plant in Tonopah, Nevada, USA, with 10 h of thermal storage in ~32000 tons solar salt (source: SolarReserve)

attractive to raise the upper operation temperature to > 550 °C in order to increase the efficiency of the power cycle. Table 1 compares the thermophysical properties and large-scale prices of commonly considered molten salts as TES and HTF materials in CSP. From the comparison, it can be concluded that: (1) commercial nitrate/nitrite salts have high heat capacities and low prices, but low thermal stability limits (decomposed at ~550 °C); (2) carbonate salts have high thermal stability limits (stable > 650 °C) and high heat capacities, but high prices particularly when containing expensive Li_2CO_3; (3) fluoride salts have high thermal stability limits (stable > 700 °C) and high heat capacities, but are toxic and expensive; (4) chloride salts have high thermal stability limits (stable > 800 °C), moderate heat capacities, and low prices.

Regarding the thermophysical properties and large-scale prices, chloride salts containing $MgCl_2$ or $ZnCl_2$ have been identified to be one of the most promising TES and HTF materials in the next generation CSP defined by US Department of Energy, combining the supercritical carbon dioxide (sCO_2) Brayton cycle ($T > 720$ °C) for increasing thermo-electric conversion efficiency (see Fig. 4) [4]. However, the high operating temperature of chloride salt mixtures causes additional challenges, particularly increase corrosiveness of structural alloys in the containers and tubes [4,11,12]. Addition of $MgCl_2$ or $ZnCl_2$ in

Fig. 3 A molten salt storage tank (container) for the Crescent Dunes solar power plant. Size of tank: 12.2 m tall and 42.7 m in diameter; storage capacity: 32000 tons molten salt (source: SolarReserve)

Table 1 Properties and prices of commonly used molten salts as TES/HTF in CSP

Molten salts composition/ wt-%	Melting point / °C	Stability limit / °C	Density / ($g \cdot cm^{-3}$)	Heat capacity /(kJ $\cdot kg^{-1} \cdot K^{-1}$)	Material cost / (US \$ $\cdot kg^{-1}$)
Solar salt $KNO_3/nANO_3$ (40/60)	240 [8]	530–565 [8]	~1.8 [8] (400 °C)	~1.5 [8] (400 °C)	0.8 [4], 0.5 [7]
Hitec $KNO_3/NaNO_3/NaNO_2$ (53/7/40)	142 [8]	450–540 [8]	~1.8 [8] (400 °C)	1.5 [8] (400 °C)	0.9 [7]
LiNaK carbonates K_2CO_3/ Li_2CO_3/Na_2CO_3 (32/35/33)	397 [8]	> 650 [8]	2.0 [8] (700 °C)	1.9 [8] (700 °C)	2.5 [4], ~1.3 [7]
LiNaK fluorides KF/LiF/NaF (59/29/12)	454 [8]	> 700 [8]	2.0 [8] (700 °C)	1.9 [8] (700 °C)	> 2*
ZnNaK chlorides $KCl/NaCl/ZnCl_2$ (23.9/7.5/68.6)	204 [7]	850 [7]	~2.0 [9] (600 °C)	0.8 [7] (300–600 °C)	0.8 [4], < 1 [7]
MgNaK chlorides $KCl/MgCl_2/NaCl$ (17.8/68.2/14.0)	380 [10]	> 800 [4]	~1.7 [9] (600 °C)	~1.0 [9] (500–800 °C)	< 0.35 [4]

*The prices are estimated with the approximate large-scale prices for salts

chloride salt mixtures leads to low melting points. However, $MgCl_2$ and $ZnCl_2$ are strongly hydrophilic chlorides. A small amount of inherent water leads to a severe corrosion of alloys in the molten chlorides [4,11]. Thus, studies on decomposition and purification of hydrophilic chlorides, and on corrosion behaviors and mechanisms of alloys in molten chlorides at high operating temperatures (500–800 °C), are essential to realize the applications of molten chlorides in CSP and high-temperature industrial processes [1,4].

Reviews on corrosion of metallic alloys in molten salts at high temperatures have been published in several books, e.g., in molten nitrates/nitrites, carbonates, sulphates [13,14] and molten chlorides [14]. Moreover, to assist the corrosion control, the use of electrochemical techniques such as polarization curves was introduced to study and monitor steel corrosion in molten salts [13]. Currently, Patel et al. [15] reviewed the results of recent studies on compatibility of molten salts (fluorides, nitrates, chlorides, sulphates, carbonates) with the structural alloys and materials. Emphasis of this review [15] was also given on corrosion kinetics of the structural alloys and materials

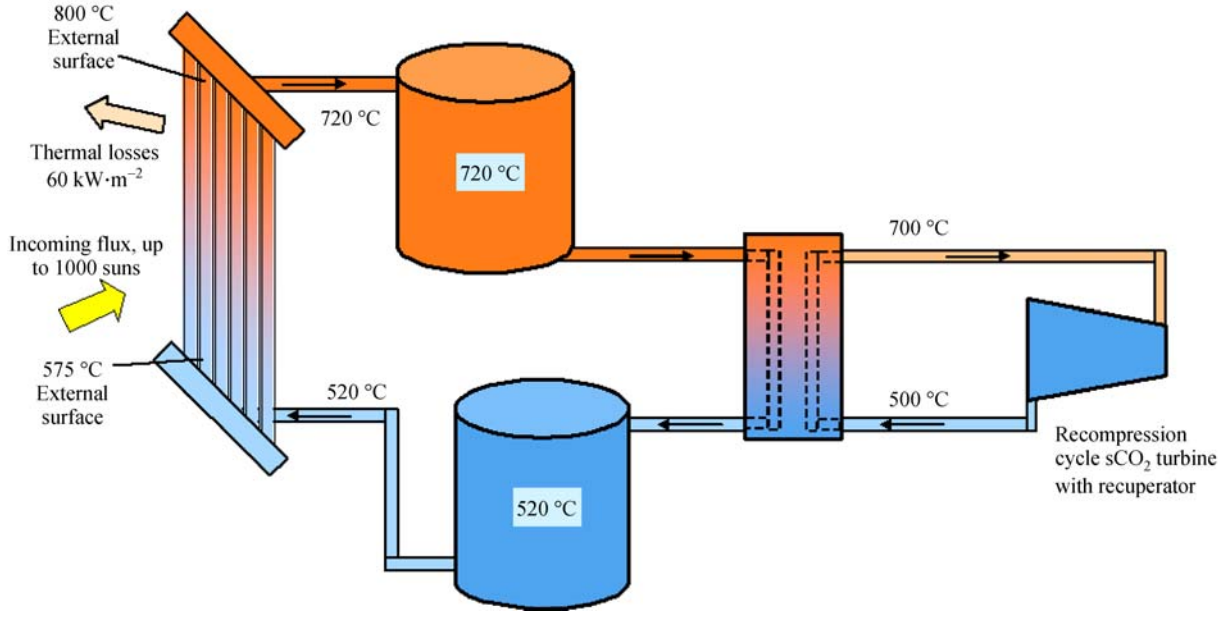

Fig. 4 High temperature molten salt loop schematic with potential surface and fluid temperatures [4]. Adapted from Concentrating Solar Power Gen3 Demonstration Roadmap of NREL, USA

in these molten salts with focus on reaction mechanisms and corrosion products. However, all the publications above did not give in-depth insight into the effect of corrosive impurities in molten chloride salts and atmosphere over molten chloride salts on the corrosion rates of alloys. To our best knowledge, a review focusing on corrosion studies of alloys in molten chlorides is also not available.

Corrosion of metallic alloys in molten chlorides consists of: (1) interaction of chloride melts with covering gases (i.e., atmosphere), (2) reactions in chloride melts and (3) interaction of metallic alloys with chloride melts. Thus, the first part of this review discusses the interaction of chloride melts with covering gases (Chapter 2). Then, decomposition and purification of chloride salts with hydrated water (impurities production during heating and its suppression), as well as a novel electrochemical technique developed by DLR to *in-situ* monitor corrosive impurities remaining in molten chlorides are introduced in Chapter 3. Finally, Chapter 4 reviews corrosion rates and mechanisms of various alloys in molten chlorides under various conditions, as well as a brief introduction of corrosion mitigation methods available in literature.

2 Interaction of chloride melts with gases

In the molten salt storage tanks for TES, the molten salts are covered with a covering gas for salt stabilization (e.g., air for nitrates/nitrites, CO_2 containing gases for carbonates), or to avoid intake of corrosive gases such as O_2 and water vapor from the atmosphere (e.g., inert gases like argon for chlorides).

Table 2 summarizes the solubilities of gases O_2, H_2O, HCl, Cl_2 and CO_2 in molten chlorides (H_2 in molten fluorides) and their interaction with molten chlorides. The gases O_2, H_2O, HCl, Cl_2, CO_2 and H_2 possess a low solubility in molten alkali and alkaline-earth chlorides/fluorides [12,16]. At 850–925 °C, the solubility constants (i.e., Henry's law constant) of H_2O, HCl, Cl_2 and CO_2 in single chlorides or chloride mixtures are in the range of 10^{-2} to 1 $mol \cdot cm^{-3} \cdot Pa$, while O_2 has an even smaller solubility constant of ~10^{-3} $mol \cdot cm^{-3} \cdot Pa$ [12]. The solubility constant of H_2 in molten LiF-BeF_2 (66–34 mol-%) at 600 °C is 4.3×10^{-3} $mol \cdot cm^{-3} \cdot Pa$ [16]. In spite of low solubilities, the oxidizing gases O_2 and H_2O dissolved in molten chlorides cause a significant metal corrosion even if the metal has no direct contact with the gases [12]. As shown in Table 2 and reactions (1–2), the oxygen gas [12,17] and water vapor [4,11,18] can react with the molten chlorides to form Cl_2 and HCl.

Chlorination :

$$4Cl^-(l) + O_2(g) \rightarrow 2Cl_2(g) + 2O^{2-}(l) \quad (1)$$

Hydrolysis :

$$H_2O(g) + Cl^-(l) \rightarrow HCl(g) + OH^-(l) \quad (2)$$

Although the equilibrium constant of reaction (1) at 700–900 °C is 10^{-25}–10^{-29} and the concentrations of Cl_2

Table 2 Gas solubilities in molten halides and gas interaction with pure molten chlorides.

Gases	O_2	H_2O	HCl	Cl_2	CO_2	H_2
Henry's law constant /(10^{12} mol·cm^{-3}·Pa^{-1})	~10^{-3} (chlorides) [12]	0.95 (NaCl, 900 °C) [16] 1.1 (KCl, 900 °C) [16]	0.13 (NaCl, 907 °C) [16] 0.25 (KCl, 907 °C) [16] 8.4×10^{-2} ($MgCl_2$, 904 °C) [16] 0.2 ($MgCl_2$/KCl, 50/50 mol-%, 875 °C) [16]	5.4×10^{-2} (NaCl, 900 °C) [16] 0.19 (KCl, 900 °C) [16] 7.3×10^{-2} ($MgCl_2$, 925 °C) [16] 3.4×10^{-2} ($MgCl_2$/NaCl/KCl, 50/27.7/23.3 wt-%, 903 °C) [16]	6.19×10^{-2} (NaCl, 904 °C) [16] 7.9×10^{-2} (KCl, 903 °C) [16] 0.36 ($MgCl_2$, 850 °C) [16]	4.3×10^{-3} (LiF-BeF_2, 66–34 mol-%, 600 °C) [16]
Interaction	Yes [12,17] Chlorination $4Cl^-(l) + O_2(l,g) \rightarrow 2Cl_2(l,g) + 2O^{2-}(l)$	Yes [11,18] Hydrolysis $H_2O(l,g) + Cl^-(l) \rightarrow HCl(l,g) + OH^-(l)$	–	–	–	–

and of O^{2-} in the melts have to be very low [12], the chlorination reaction can be enhanced, if such cations as Zn^{2+}, Mg^{2+}, Al^{3+}, Fe^{2+}, Cr^{2+}, Ni^{2+}, etc., which can form low-solubility oxides with oxygen ions [12,17], are present in the melts. Moreover, if these cations can form stable metal-hydroxyl ions (e.g., $MgOH^+$) in the melts with hydroxyl ions [11,18], the hydrolysis reaction (reaction (2)) can be shifted to the right side. The reaction products Cl_2 and HCl as well as metal-hydroxyl ions have higher solubilities than O_2 in molten chlorides, which leads to an enhanced metal corrosion even if the metal has no direct contact with the gases. Thus, in order to control corrosion of alloys in molten chlorides for a long lifetime of CSP, the intake of O_2 and H_2O from the atmosphere and presence of O_2 and H_2O in the covering gases should be avoided. Moreover, the chloride salts with adsorbed O_2 and H_2O should be purified.

3 Impurities in chloride melts

3.1 Decomposition and purification of hydrophilic chlorides

Effort to reduce corrosiveness of the molten chloride salts with hydrophilic chlorides has been made to reduce the corrosive impurities by suppressing the side reactions of hydrolysis during the salt heating [18–20]. In this review, the decomposition and purification of $MgCl_2$ is discussed as an example to understand the decomposition and purification of chlorides.

Maksoud and Bauer [18] have investigated the purification of a $MgCl_2$-NaCl-KCl salt mixture (60-20-20 mol-%, melting temperature of ~400 °C) containing hydrated $MgCl_2$ ($MgCl_2 \cdot 6H_2O$) via thermal analysis (differential scanning calorimetry/thermogravimetric analysis) coupled to mass spectrometry, salt analysis (X-ray diffraction (XRD)) and monitoring produced HCl gas (pH-value analysis of the wash water with a pH electrode). In their work, an advanced process technology and purification approach (i.e., sweeping the salt with inert gas during the heating and keeping the temperature at 350 °C before heating above the melting point until the salt is completely dehydrated) has been developed yielding improved salt quality with less impurities like corrosive MgOHCl and HCl and thus reduce corrosiveness [18]. Kipouros and Sadoway [19] used multi-step heating to purify the hydrated $MgCl_2$ according to a vapor pressure diagram of H_2O and HCl over the hydrates of $MgCl_2$ (see Fig. 5). As shown in Fig. 5, with the temperature increasing, the hydrophilic $MgCl_2$ at room temperature — $MgCl_2 \cdot 6H_2O$ was dehydrated to $MgCl_2 \cdot 4H_2O$ at T_1, to $MgCl_2 \cdot 2H_2O$ at T_2 and to $MgCl_2 \cdot H_2O$ at T_3, sequentially [19]. In order to reduce the side reaction of $MgCl_2 \cdot 2H_2O$ to MgOHCl and HCl (see reaction (3)) and release more water vapor, the temperature was controlled between T_3 and T_4, until all the $MgCl_2 \cdot 2H_2O$ is dehydrated to $MgCl_2 \cdot H_2O$ [19]. At the temperature higher than T_4, the side reactions of $MgCl_2 \cdot H_2O$ and $MgCl_2 \cdot 2H_2O$ to MgOHCl and HCl (see reactions (3) and (4)) can take place before the target reaction of $MgCl_2 \cdot H_2O$ to $MgCl_2$ at T_5 [19]. These side reactions were averted by increasing the partial pressure of HCl in the gas around the salt, e.g., by sweeping the salt with HCl [19].

$$MgCl_2 \cdot 2H_2O \rightarrow MgOHCl + HCl + H_2O \quad (3)$$

$$MgCl_2 \cdot H_2O \rightarrow MgOHCl + HCl \quad (4)$$

However, even after salt purifications [18–20], still a small amount of hydroxide impurities remains in the salts. The formed MgOHCl can be dissolved in the molten chlorides (to $MgOH^+$ and Cl^-) and decomposes further to MgO and corrosive HCl at high temperatures (> 555 °C) [19]. Thus, metal-hydroxyl chloride salts such as MgOHCl are considered to be the most critical corrosive impurities in molten chlorides containing hydrophilic chlorides under inert atmosphere.

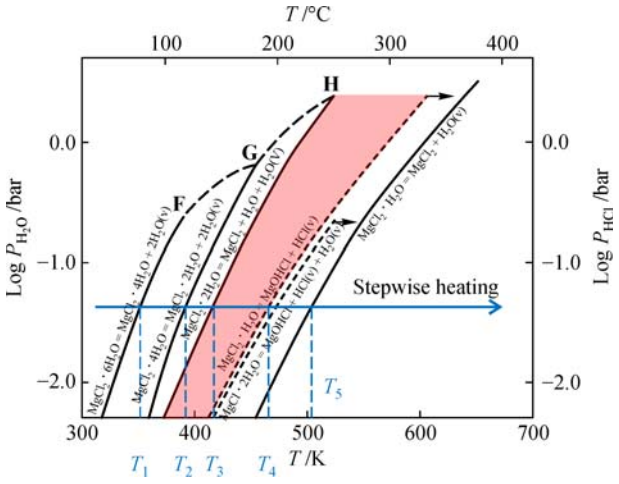

Fig. 5 Vapor pressure of H_2O and HCl over the hydrates of $MgCl_2$ [19]

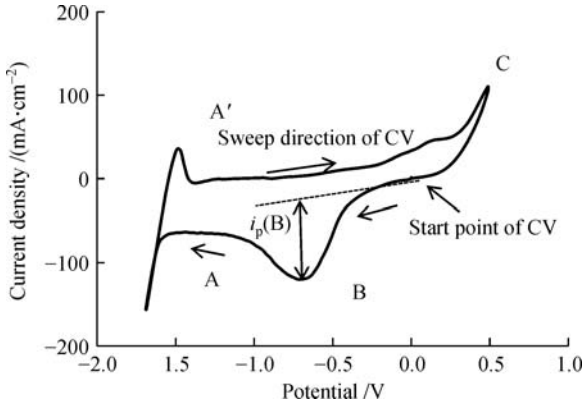

Fig. 6 Cyclic voltammogram in $MgCl_2$/KCl/NaCl at 500 °C obtained by a tungsten working electrode. Sweep rate: 200 mV·s^{-1}. Tungsten reference electrode. i_p(B): peak current density for reaction B. Adopted from [24]

3.2 Cyclic voltammetry to *in-situ* monitor corrosive impurities

Cyclic voltammetry (CV) has been used to analyze the electrochemistry of molten chlorides, e.g., $MgCl_2$/NaCl (730–850 °C) for measuring hydroxide/oxide impurities [21], or LiCl/KCl/$TiCl_2$ (430–500 °C) for the synthesis of Ti alloys [22]. For an efficient control of corrosive impurity concentrations in molten chloride salts, earlier studies conducted by the authors of this review [23–25] used CV to *in-situ* measure the corrosive impurities in molten chlorides, e.g., hydroxide containing ion $MgOH^+$ in molten NaCl-KCl-$MgCl_2$. Compared to the *ex-situ* methods such as titration [21,24], generally *via* collecting and analyzing a salt sample out of the melt, *in-situ* measurements of the impurities such as hydroxide containing ions with an electrochemical analytic system based on CV provide unique possibility to monitor impurity concentrations and thus control the technological processes [21,24].

It was found that in melts such as $MgCl_2$-NaCl [21], NaCl-KCl [26], $MgCl_2$-KCl [26], LiCl-KCl [26], $CaCl_2$-CaO [27], $CaCl_2$-KCl [28], the heights of the reduction peaks of hydroxide/oxide species in cyclic voltammograms were directly proportional to the concentrations of hydroxide/oxide species. This phenomenon was also observed by the CV experiments in our studies [23–25] for the concentration of $MgOH^+$ corrosive impurity in molten NaCl-KCl-$MgCl_2$ (60/20/20 mol-%) salts at temperatures of 500–700 °C. A typical cyclic voltammogram by using the tungsten working electrode [24] is shown in Fig. 6. The peak B was considered to represent the following electrochemical reaction [24]:

$$\text{Reaction B}: MgOH^+ + e^- = MgO(s) + \frac{1}{2}H_2(g) \quad (5)$$

By fitting the CV data with those from the acid consumption measurements (i.e., titration) on the simultaneously collected salt samples, it was found that the peak current density of the peak B (i_p(B)) was proportional to the bulk concentration of $MgOH^+$ ($c^\infty(MgOH^+)$) in the studied temperature range, i.e., at 500–700 °C [23–25]:

$$i_p(B) = k(T,v)(B)\cdot c^\infty(MgOH^+), \quad (6)$$

where i_p represents the peak current density in mA·cm^{-2}; $k(T,v)$ is a constant, i.e., the slope of peak current densities *vs.* concentrations of the reacting species in (10^{-4} wt-% O)/(mA·cm^{-2}), which depends on the temperature T and v potential sweep rate; c^∞ is the bulk concentration of the reacting species in 10^{-4} wt-% O. As shown in Fig. 7 from [25], the slope rates of current densities *vs.* concentrations of $MgOH^+$ at 500–700 °C were determined, which compare well with literature [21]. Thus, the peak current densities of the peak B obtained via CV could simply be used to *in-situ* monitor the concentration of the hydroxide impurity in the molten NaCl-KCl-$MgCl_2$ [25]. This method may be extended to other molten chloride salts with hydroxide impurity or other impurities.

4 Corrosion of alloys in molten chlorides

4.1 Corrosion rates of alloys in molten chlorides

As molten chlorides are promising TES and HTF materials in the next generation CSP regarding their thermal properties and prices [4], corrosion behaviors of alloys in them have been investigated intensively in the last years (e.g., starting with the work in the US SunShot Initiative). Table 3 summarizes the corrosion rates of various alloys (stainless steels, nickel-based superalloys, some model alloys) in molten chloride mixtures under various conditions (e.g., various temperatures, under oxidizing or inert atmosphere) [14,29–35].

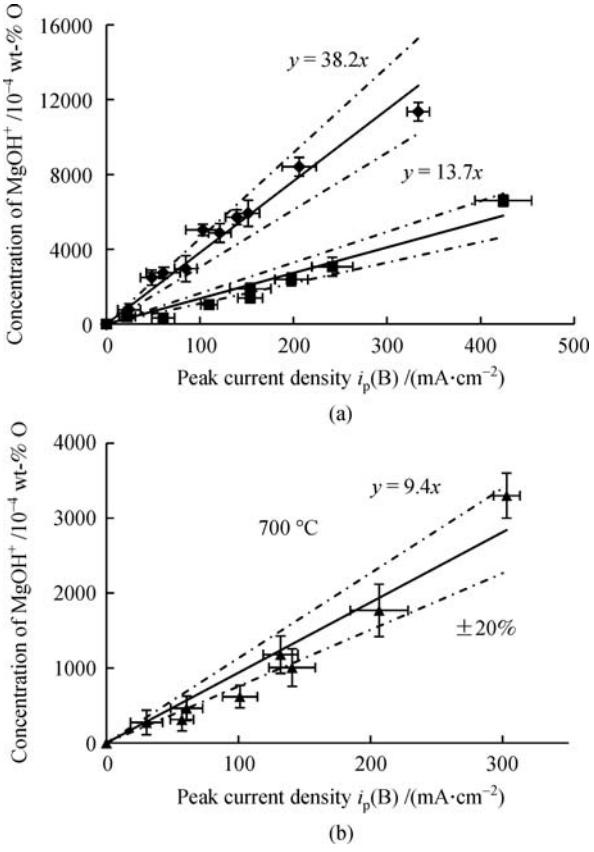

Fig. 7 Peak current densities *vs*. concentrations of corrosive $MgOH^+$ in molten $MgCl_2$/KCl/NaCl (60/20/20 mol-%) at (a) 500, 600 °C and (b) 700 °C. Error bars represent the standard deviations in the CV (three measurements) and AC measurements (three measurements). Adopted from [24]

The corrosion rates (*CR*) were conventionally determined with a mass loss measurement (referred to method "I + M") or microstructural analysis (referred to method "I + MS") on the exposed alloy specimens after immersion tests in the melts according to the following equations [14,29]:

$$\text{method "I + M"}: CR = \frac{\Delta m}{\rho \cdot A} \cdot \frac{365 \cdot 24}{t} \cdot 10^4, \quad (7)$$

$$\text{method "I + M"}: CR = S_{\text{corr}} \cdot \frac{365 \cdot 24}{t}, \quad (8)$$

where *CR* has the unit of μm·year^{-1}; Δm is the mass change of the exposed alloy specimen after immersion test, g; ρ is the density of the exposed alloy specimen, g·cm^{-3}; *A* is the contact area of the exposed alloy specimen with the melt, cm^2; *t* is the immersion time, h; S_{corr} is the thickness of the corrosion layer of the exposed alloy specimen, μm.

Besides these post-analysis methods (methods "I + M" and "I + MS"), the electrochemical techniques such as potentiodynamic polarization (PDP) [30–32,34,35] and electrochemical impedance spectroscopy (EIS) (for alloys in KCl/$MgCl_2$ at 550–700 °C [36]) were used for *in-situ* and fast measurements of the corrosion rates. The corrosion current obtained with the electrochemical techniques can be used to calculate an estimated corrosion rate according to Faraday law [14,30–32]:

$$CR = k[I_{\text{corr}} \cdot EW / \rho \cdot A], \quad (9)$$

where the corrosion rate (*CR*) has the unit of μm per year, *k* = 3.27 in μm·g·μA^{-1}·cm^{-1}·year^{-1}, I_{corr} is the corrosion current in μA, *A* is the contact area of the working electrode (studied alloys) with molten chlorides, *EW* and ρ are the equivalent weight (dimensionless) and density (g·cm^{-3}) of the alloy sample, respectively [31].

Compared to the conventional immersion methods, which generally require several immersion days to detect the mass loss and microstructural change of the exposed alloy specimens, the electrochemical techniques can give indicative corrosion rates of alloys within several minutes. Thus, they can be used for parametric studies of corrosion rates of alloys. Compared to PDP and EIS, post analysis on the exposed alloy specimens after immersion tests can provide more information on the corrosion layers and mechanisms by analyzing the corrosion products and microstructures of the exposed alloys.

From Table 3, it can be concluded that the temperature of molten chlorides and the atmosphere (with or without oxidizing species) above the molten chlorides have significant effect on the corrosion of alloys in molten chlorides. The corrosion rates of alloys in molten chloride mixtures increase with increasing temperature, significantly, in particular above 600 °C. For instance, the corrosion rate of Ha C-276 in molten $ZnCl_2$-NaCl-KCl under air increased more than 10-fold (from 40 to 500 μm·year^{-1}), when the temperature increased from 500 to 800 °C [31].

As oxidizing species O_2 and H_2O existing in air as covering gas can accelerate the corrosion of alloys. Alloys in molten chlorides have much higher corrosion rates under air atmosphere than under inert atmosphere, e.g., SS 304, Ha C-22 and Ha C-276 in molten $ZnCl_2$-NaCl-KCl [31]. However, severe corrosion occurred also in inert atmosphere, e.g., SS and incoloy alloys in molten NaCl-KCl under nitrogen atmosphere at 650–700 °C [32], SS alloys in molten KCl/NaCl/VCl_2 under argon atmosphere [34], if corrosive species such as O_2, H_2O, V^{2+} exists in the melts. Moreover, it was concluded that molten chlorides were too aggressive to be used at 900 °C under the atmosphere with O_2 and H_2O, and reducing these oxidizing impurities in molten chlorides can also significantly reduce the corrosiveness of the molten chlorides [14].

For the corrosion behavior of commercial alloys in molten nitrate salt mixtures such as solar salt it is well understood, that the corrosion resistance of alloys to molten nitrate salt mixtures improves with increasing

Table 3 Results of corrosion studies metallic alloys in molten chlorides[a)]

Molten salts /wt-%	Alloy /Ni wt-%	T /°C	Atmosphere	Method	Corrosion rate /(μm·year^{-1})	Ref.
$KCl/NaCl/ZnCl_2$ (24.0/7.4/68.6)	Ha N (~71)	250	Air	PDP	37	[30]
		500	Air	PDP	160	[30]
	Ha C-22 (~56)	250	Air	PDP	16	[30]
		500	Air	PDP	50	[30]
	Ha C-276 (~57)	250	Air	PDP	11	[30]
		500	Air	PDP	42	[30]
	SS 304 (8–11)	250	Air	PDP	22	[31]
		500	Air	PDP	381	[31]
		400	Absence of air	I + M (1000 h)	14	[31]
	Ha C-22 (~56)	250	Air	PDP	15	[31]
		500	Air	PDP	42	[31]
		400	Absence of air	I + M (1000 h)	8	[31]
		800	Absence of air	I + M (1000 h)	14	[31]
	Ha C-276 (~57)	500	Air	PDP	40	[31]
		800	Air	PDP	500	[31]
		400	Absence of air	I + M (1000 h)	3	[31]
		800	Absence of air	I + M (1000 h)	4	[31]
		500	Air	I + M (1000 h)	80	[31]
$CaCl_2/MgCl_2/NaCl$ (43.6/17.7/38.7)	Inc 625 (~62)	600	Air	I + M (504 h)	121	[29]
	Ha X (~47)	600	Air	I + M (504 h)	153	[29]
	Ha B-3 (~65)	600	Air	I + M (504 h)	144	[29]
$KCl/MgCl_2/NaCl$ (20.4/55.1/24.5)	SS 304 (8–11)	450–500	Vacuum	I + M (1000 h)	< 10	[14]
	SS 316 (10–14)	450–500	Vacuum	I + M (1000 h)	~10	[14]
	SS 347 (9–12)	450–500	Vacuum	I + M (1000 h)	~120	[14]
	Ha N (~71)	450–500	Vacuum	I + M (1000 h)	~50	[14]
	SS 304 (8–11)	900	N_2-(0.1–1%H_2O)-(1–10%O_2)	I + M (144 h)	Disintegrated	[14]
	SS 316 (10–14)	900	N_2-(0.1–1%H_2O)-(1–10%O_2)	I + M (144 h)	Disintegrated	[14]
	In 800H (30–35)	900	N_2-(0.1–1%H_2O)-(1–10%O_2)	I + M (144 h)	23725	[14]
	Ha 230 (~57)	900	N_2-(0.1–1%H_2O)-(1–10%O_2)	I + M (144 h)	20345	[14]
$KCl/NaCl/VCl_2$ (53.3/41.7/5.0)	SS 316L (13.5–15.0)	750	Argon	I + M (6 h)	54000	[34]
		750	Argon	PDP (6 h)	1600	[34]
	SS 316Ti (12–14)	750	Argon	I + M (6 h)	61000	[34]
		750	Argon	PDP (6 h)	7000	[34]
	SS 321 (9–11)	750	Argon	I + M (6 h)	22200	[34]
		750	Argon	PDP (6 h)	15100	[34]
KCl/NaCl (56.1/43.9)	SS 316L (13.5–15.0)	750	Argon	I + M (80 h)	~157	[35]
	SS 316Ti (12–14)	750	Argon	I + M (80 h)	~168	[35]
	SS 321 (9–11)	750	Argon	I + M (80 h)	~225	[35]
KCl/LiCl (55.8/44.2)	SS 304 (8–11)	400	Absence of air	I + M (–)	2	[14]
		500	Absence of air	I + M (–)	6	[14]
	SS 316 (10–14)	400	Absence of air	I + M (–)	2	[14]
	SS 347 (9–12)	500	Absence of air	I + M (–)	2	[14]

(*Continued*)

Molten salts /wt-%	Alloy /Ni wt-%	*T* /°C	Atmosphere	Method	Corrosion rate /(μm·year^{-1})	Ref.
LiCl/NaCl (68.6/34.4)	SS 347 (9–12)	650	Nitrogen	PDP	7490	[32]
	SS 310 (~20.5)	650	Nitrogen	PDP	6420	[32]
		700	Nitrogen	PDP	12450	[32]
	In 800H (30–35)	650	Nitrogen	PDP	5940	[32]
		700	Nitrogen	PDP	14310	[32]
	Inc 625 (~62)	650	Nitrogen	PDP	2800	[32]
$MgCl_2$/NaCl (52/48)	Ni (> 99.97)	520	Air	I + M (140 h)	57	[33]
	GH 4033 (Ni72.1/Cr20.5/ Fe4.0/Ti2.6/Al0.8)	520	Air	I + M (140 h)	142	[33]
	GH 4169 (Ni52.9/Cr19.0/ Fe18.5/Ti0.9/Al0.84/Mo3.1/ Nb5.2)	520	Air	I + M (140 h)	246	[33]

a) SS: stainless steel; Ha: hastelloy; In: incoloy (Ni wt-% < 50%); Inc: inconel (Ni wt-% > 50%); PDP: potentiodynamic polarization. I + M (immersion time): immersion test + mass loss. I + MS (immersion time): immersion test + microstructural analysis

nickel content [14]. From the available corrosion data in literature for alloys in molten chlorides summarized in Table 3, it can be concluded that nickel-based superalloys such as incoloy, inconel and hastelloy, which have higher prices due to higher Ni contents, mostly have better corrosion resistance in molten chloride salts than stainless steels [32,33]. However, the conclusion that the resistance of alloys improves with increasing nickel content, is not always true for alloys to molten chlorides. In some cases, the alloys with higher Ni-content have worse corrosion resistance, e.g., Ha N (~71% nickel) has higher corrosion rates in molten $ZnCl_2$-NaCl-KCl than Ha C-22 (~56% nickel) and Ha C-276 (~57% nickel) at 250–500 °C [30], also in NaCl-KCl-$MgCl_2$ than SS 304 (8%–11% nickel) and SS 316 (10%–14% nickel) at 450–500 °C [14]. Ha N has been found to be most suitable in molten fluoride salts after extensive studies for nuclear applications at temperatures of >700 °C under vacuum or an inert atmosphere [14]. However, other studies [14,30] indicate that Ha N is not suitable for molten chloride salts under air or vacuum.

4.2 Interaction of chloride melts with metallic alloys

Corrosion mechanisms of metallic alloys in molten chloride salts are complex with different interactions between atmosphere, molten salts, outer corrosion layer, inner corrosion layer and the matrix of metallic alloys [17,29,33,37]. The interaction between atmosphere (covering gases) and molten chlorides has been discussed in section 2.2. In this section, the interaction between molten chlorides with corrosive impurities (e.g., O_2, Cl_2, HCl, OH^- containing species) and metallic alloys is discussed by reviewing the available literature [17,29,33,35,37].

As summarized in Table 4, research efforts have been made to understand the corrosion mechanism of metallic alloys in molten chloride salts under oxidizing [17,29,33,37] or inert [35] atmosphere. Analysis methods like scanning electron microscopy (SEM), energy dispersive spectroscopy (EDS), XRD, electronic adsorption spectroscopy (EAS) and electrochemical methods like open circuit potential (OCP), linear voltammetry (LV), electrochemical impedance spectroscopy (EIS) were used to analyze the corroded alloys, corrosion products and corrosion behaviors (see Table 4). It can be concluded that the interaction between molten chlorides with corrosive impurities and metallic alloys has two stages (see Fig. 8): (1) oxidation of elements in alloys, (2) dissolution, precipitation and/or vaporization of oxidized metallic elements. As shown in Table 5, the alloying element M, e.g., Cr, which has a stronger electromotive force [38], i.e., lower standard electrode potential in molten chlorides [39], reacts with oxidizing impurities faster. Thus, in theory, the alloying elements (Al, Mn, Cr, Fe, Ni) oxidized by oxidizing impurities in molten chlorides (e.g., O_2, Cl_2, HCl, OH^- containing species) to metallic ions tend to be depleted from alloys according to the sequence of Al > Mn > Cr > Fe > Ni. This phenomenon has been observed and reported in different studies [17,29,33,35,37]. The metallic ions dissolved in the molten chlorides interact with the ions in the melt further to form, e.g., stable chloride ions $M_xCl_y^{z-}/M_xCl_y^{z+}$, oxide precipitates M_xO_y, gases $M_xCl_y/M_xCl_yO_z$, which can enhance the oxidation reactions of the alloying elements with the oxidizing impurities in the molten chlorides (stage 1) [17,29,33,35,37].

Liu et al. [29] investigated the corrosion mechanism of commercial Ni-based (Ni-Cr-Fe) superalloys in molten $MgCl_2/CaCl_2$/NaCl under air atmosphere at 600 °C by analyzing the corroded alloys via SEM and EDS and

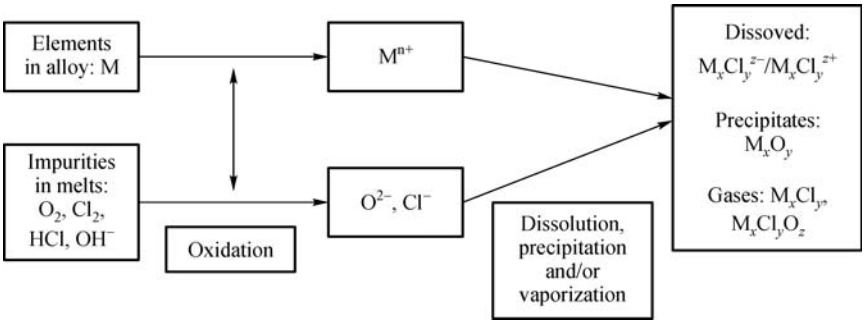

Fig. 8 Interaction between molten chlorides with corrosive impurities and metallic alloys

Table 4 Corrosion of metallic alloys in molten chlorides[a)]

Molten chlorides /wt-%	Alloys	Atmosphere temperature /°C	Procedures	Corrosion mechanism	Ref.
$CaCl_2/MgCl_2/NaCl$ (43.6/17.7/38.7)	Ni-based commercial superalloys	Air /600	SEM, EDS, XRD, TC	Preferential depletion of Cr and Fe, intergranular corrosion	[29]
$MgCl_2/NaCl$ (52/48)	Ni-based alloys (Ni 52.9–99.97 wt-%)	Air /520	SEM, EDS, XRD	Combined effect of alloy dissolved as anode, preferential oxidization and chlorination	[33]
KCl/NaCl (56.1/43.9)	Stainless steels	Argon /750	EAS, XRM, SEM, OCP, LV, EIS	Intergranular corrosion, preferential depletion of Cr, Fe and Mn	[35]
KCl-$ZnCl_2$ (69.1/30.9)	NiAl and FeAl model alloys	Air /400–450	SEM, EDX, XRD, EPMA	Preferential depletion of Al, formation of Al_2O_3 within the pores of corrosion layer	[17]
$MgCl_2/NaCl$ ($MgCl_2$ wt-% 0.0, 48.9, 61.0, 93.6)	GH 1140 (Ni37.5/Cr21.5/Fe35.85/ Ti0.9/Al0.4/Mo2.25/ W1.6)	Air /850	SEM, EDS, XRD	Without $MgCl_2$: dissolution as anode–oxidizing–peeling off of oxide film, with $MgCl_2$: dissolution as anode–oxidation–reduction–peeling off of oxide film	[37]

a) TC: thermodynamic calculation; XRM: X-ray microanalysis; EDX: energy-dispersive analysis; EPMA: electron probe microananlysis

corrosion products via XRD, as well as based on the TC of corrosion reactions. The combined effect of dissolution, oxidization and chlorination was considered in the corrosion mechanism of alloys in molten chlorides [29]. During the exposure, oxygen and water in air were continuously dissolved in the molten chlorides and reacted with the molten chlorides to form corrosive HCl and Cl_2. These corrosive impurities could accelerate the corrosion of alloys, particularly the Cr element in the alloys, which has lower standard electrode potential in molten chlorides compared to Fe and Ni [39] (see Table 5). In this system, gases like $CrCl_4$ and CrO_2Cl_2, and oxide precipitates like $MgCr_2O_4$ and MgO were considered to be the main products of corrosion reactions based on the thermodynamic calculation [29]. Wang et al. [37] investigated the influence of $MgCl_2$ content on corrosion behavior of metallic alloys in $MgCl_2/NaCl$ under air atmosphere at 850 °C. It was found that corrosion mechanisms were different with or without $MgCl_2$ in molten chlorides. With $MgCl_2$, a MgO layer was formed on the alloy surface but could not protect the alloy against corrosion due to its porous structure and peeling off from the alloy surface [37].

Abramov et al. [34] studied corrosion mechanisms of stainless steels (SS 316L, 316Ti and 321) in molten KCl/NaCl under inert atmosphere at 750 °C by analyzing the molten salts and corroded alloys via EAS, SEM, XRM, as well as using electrochemical methods like OCP. The dissolution sequence of the alloying elements was determined by combination of EAS for melts with consecutive chemical analysis of quenched melts. Fe, Cr and Mn species were in the major products of the anodic

Table 5 Standard electrode potentials of metallic elements in molten $MgCl_2$/KCl/NaCl (50/20/30 mol-%) at 475 °C [39]

Elements	Al	Mn	Cr	Fe	Ni
E^0_m /V *vs.* Pt^{2+}/Pt	−1.886 (Al^{3+}/Al)	−1.794 (Mn^{2+}/Mn)	−1.396 (Cr^{2+}/Cr) −1.131 (Cr^{3+}/Cr)	−1.183 (Fe^{2+}/Fe) −0.852 (Fe^{3+}/Fe)	−0.792 (Ni^{2+}/Ni)

dissolution of these studied stainless steels [35]. Moreover, intergranular corrosion of these studied stainless steels in molten chlorides was characterized by electrochemical methods like OCP measurements [35].

Table 3 clearly shows the difficulty to control the corrosion rates of alloys exposed to molten chlorides under oxidizing atmosphere below 15 μm·year^{-1} ($\geqslant$600 °C), due to the effect of oxidizing species like O_2 and H_2O. Compared to oxidizing atmosphere, the alloys have much lower corrosion rates when exposed to the molten chlorides under inert atmosphere. However, there is still a lack of reliable data and research on the corrosion rates and mechanism of metallic alloys in molten chlorides under inert atmosphere. Thus, more research is essential to cover this gap for realizing the application of molten chlorides in CSP.

4.3 Corrosion mitigation methods

Some methods like adding corrosion inhibitors [40–42] in the melts or forming a protective layer on alloys [36, 43–45] have been studied to mitigate the corrosion rates of metallic alloys in molten chlorides at high temperatures.

Cathodic protection is a well-known method for preventing metallic corrosion in aqueous solutions to the previous alloy corrosion potential, either by using impressed current or by using a sacrificial anode. The protection method of using a sacrificial anode has been used to reduce the corrosiveness of the molten chloride salts by saturation of a salt with a liquid metal (i.e., LiCl with Li metal [40,41]), or adding active metals such as Mg [42] in the molten chlorides, to reduce the redox potential of the melts, i.e., the concentration of the corrosive impurities like metal-hydroxyl ions and dissolved O_2/Cl_2, e.g., via the following reactions:

$$\mathrm{Mg(dissolved)} + 2\mathrm{MgOH^+} \rightarrow \mathrm{Mg^{2+}} + 2\mathrm{MgO(s)} + \frac{1}{2}\mathrm{H_2(g)} \quad (10)$$

$$2\mathrm{Mg(dissolved)} + \mathrm{O_2(dissolved)} \rightarrow 2\mathrm{MgO(s)} \quad (11)$$

$$\mathrm{Mg(dissolved)} + \mathrm{Cl_2(dissolved)} \rightarrow \mathrm{MgCl_2(l)} \quad (12)$$

The results of corrosion inhibition experiments in [42] showed that the corrosion rate of the Ni-based (Ni-Cr-Fe) superalloy Ha 230 in $MgCl_2$-KCl containing 1.15 mol-% Mg under inert atmosphere at 850 °C showed 35 times lower corrosion than baseline tests with no corrosion inhibitor and met the requirements in industrial applications (CR < 15 μm·year^{-1}). Additional experiments to aggravate corrosion by adding convective flow using a thermosiphon showed that the corrosion rate with convective flow and no Mg corrosion inhibitor increased by a factor of 3 [42], whereas thermosiphon tests with the 1.15 mol-% Mg corrosion inhibitor reduced corrosion below 15 μm·year^{-1} [42]. However, this method was not studied in real solar power applications.

Besides adding corrosion inhibitors in the melts, surface passivation by forming a protective layer on the alloys is another promising corrosion mitigation approach. Compared to the corrosion inhibitor approach, the alloy with a protective layer could be exposed to both the liquid and the vapor phases of the molten chlorides [43]. In the protective layer development for molten chlorides, research focused on: (1) ceramic layers like Al_2O_3 [36,43–45] and Yttria-stabilized zirconia [45], (2) metallic layers such as nickel based alloy coatings [44,45]. These studies showed that surface passivation by forming a protective layer on the alloys could reduce the corrosion rates of metallic alloys in molten chlorides significantly. However, there are a number of parameters to be considered for choosing an appropriate coating for a specific substrate material and environment such as corrosion environment, thermal stress (or differences in expansion coefficient of substrate and protective coating), heat resistance, dissolution of the protective layer in the melt [45].

5 Summary and conclusions

After reviewing the molten chloride development for CSP and results of studies on hot corrosion of commercial alloys in molten chlorides, it can be concluded that:

1. Molten chloride mixtures such as $MgCl_2$-KCl-NaCl are promising heat transfer fluid and thermal energy storage media for next generation CSP plants with operation temperatures up to 750 °C.

2. Molten salt temperature, atmosphere over the salt and corrosive impurities in the salt have a significant effect on corrosion rates.

3. Nickel-based superalloys such as Incoloy, Inconel and Hastelloy, which have higher prices due to higher Ni contents, typically have better corrosion resistance in molten chloride salts than stainless steels. However, the conclusion that the resistance of alloys improves with increasing nickel content, is not always true for alloys in contact with molten chlorides.

4. Corrosion of alloys in molten chlorides under air and inert atmosphere has different corrosion mechanisms due to the interaction between atmosphere and molten chlorides. This should be considered in the development of corrosion mitigation methods.

5. Corrosion rates of alloys in molten chlorides can be reduced via salt purification by, e.g., stepwise heating, as well as via corrosion mitigation methods such as adding corrosion inhibitors or forming a protective layer on alloys.

6. Electrochemical techniques like cyclic voltammetry, open circuit potential measurement, polarization curves and electrochemical impedance spectroscopy are useful tools for corrosion studies and determination of impurity levels.

The following future works, which help to realize the commercial applications of molten chlorides in next generation CSP, are suggested:

1. Corrosion study of suitable metallic structural materials for molten chlorides up to 750 °C including aspects such as corrosion in molten salt flow and thermal cycling.

2. Study on durability of the promising protective coatings on alloys.

3. Study on combining the salt purification and corrosion mitigation methods for efficient corrosion control.

4. Study on corrosion mechanism of alloys in molten chlorides with corrosion inhibitors like Mg metal.

5. Development of electrochemical techniques for commercial applications in order to monitor salt quality and corrosion.

6. Development of components and instrumentation (e.g., pumps, valves), as well as their demonstration in lab-scale molten salt test loops.

Acknowledgements This research has been performed within the DLR-DAAD fellowship programme, which is funded by German Academic Exchange Service (DAAD) and German Aerospace Center (DLR).

References

1. Minh N Q. Extraction of metals by molten salt electrolysis: Chemical fundamentals and design factors. Journal of Metals, 1985, 37(1): 28–33
2. Fray D J. Emerging molten salt technologies for metals production. Journal of the Minerals Metals & Materials Society, 2001, 53(10): 26–31
3. Wulandari W, Brooks G A, Rhamdhani M A, Monaghan B J. Magnesium: Current and alternative production routes. In: Proceedings of Chemeca 2010: Engineering at the Edge. Barton: Engineers Australia, 2010, 347–357
4. Mehos M, Turchi C, Vidal J, Wagner M, Ma Z, Ho C, Kolb W, Andraka C, Kruizenga A. Concentrating Solar Power Gen3 Demonstration Roadmap. National Renewable Energy Laboratory Technical Report NREL/TP-5500-67464. 2017
5. Kuravi S, Trahan J, Goswami D Y, Rahman M M, Stefanakos E K. Thermal energy storage technologies and systems for concentrating solar power plants. Progress in Energy and Combustion Science, 2013, 39(4): 285–319
6. Zervos A, ed. Renewables 2016: Global Status Report, 2016. Paris: REN21 Secretariat, 2016, 67–69
7. Vignarooban K, Xu X, Arvay A, Kannan H K. Heat transfer fluids for concentrating solar power systems—a review. Applied Energy, 2015, 146: 383–396
8. Lantelme F, Groult H, eds. Molten Salts Chemistry: From Lab to Applications. Amsterdam: Elsevier, 2013, 415–438
9. Li Y, Xu X, Wang X, Li P, Hao Q, Xiao B. Survey and evaluation of equations for thermophysical properties of binary/ternary eutectic salts from NaCl, KCl, $MgCl_2$, $CaCl_2$, $ZnCl_2$ for heat transfer and thermal storage fluids in CSP. Solar Energy, 2017, 152: 57–79
10. Tian Y, Zhao C Y. A review of solar collectors and thermal energy storage in solar thermal applications. Applied Energy, 2013, 104: 538–553
11. Kruizenga A M. Corrosion Mechanisms in Chloride and Carbonate Salts. SANDIA Report SAND2012-7594. 2012
12. Ozeryanaya I N. Corrosion of metals by molten salts in heat-treatment processes. Metal Science and Heat Treatment, 1985, 27 (3): 184–188
13. Sequeira C A C. High temperature corrosion in molten salts. Molten Salt Forum, 2003, 7, 117–170
14. Lai G Y, ed. High-Temperature Corrosion and Materials Applications. Ohio: ASM International, 2007, 409–421
15. Patel N S, Pavik V, Boca M. High-temperature corrosion behavior of superalloys in molten salts—a review. Critical Reviews in Solid State and Material Sciences, 2017, 42(1): 83–97
16. Tomkins R P T, Bansal N P. Gases in molten salts, a volume in IUPAC solubility data series. Oxford: Pergamon Press, 1991, Volume 45/46, 61, 114–176, 220–245, 325–339, 353–357
17. Li Y S, Spiegel M. Models describing the degradation of FeAl and NiAl alloys induced by $ZnCl_2$-KCl melt at 400–450 °C. Corrosion Science, 2004, 46(8): 2009–2023
18. Maksoud L, Bauer T. Experimental investigation of chloride molten salts for thermal energy storage applications. In: Proceedings of 10th International Conference on Molten Salt Chemistry and Technology, Shenyang, China, 2015, 273–280
19. Kipouros G J, Sadoway D R. A thermochemical analysis of the production of anhydrous $MgCl_2$. Journal of Light Metals, 2001, 1 (2): 111–117
20. Maricle D L, Hume D N. A new method for preparing hydroxide—-free alkali chloride melts. Journal of the Electrochemical Society, 1960, 107(4): 354–356
21. Skar R A. Chemical and electrochemical characterisation of oxide/hydroxide impurities in the electrolyte for magnesium production. Dissertation for the Doctoral Degree. Trondheim: Norwegian University of Science and Technology (NTNU), 2001, 26
22. Gussone J. Schmelzflusselektroytische Abscheidung von Titan auf Vertärkungsfasern zur Herstellung von Titanmatrixverbundwerkstoffen. Dissertation for the Doctoral Degree. Aachen: RWTH Aachen University, 2012, 56–80 (in German)
23. Ding W, Bonk A, Gussone J, Bauer T. Electrochemical measurement of corrosive impurities in molten chlorides for thermal energy storage. Journal of Energy Storage, 2018, 15: 408–414
24. Ding W, Bonk A, Gussone J, Bauer T. Cyclic voltammetry for monitoring corrosive impurities in molten chlorides for thermal energy storage. Energy Procedia, 2017, 135: 82–91
25. Ding W, Bonk A, Gussone J, Bauer T. Electrochemical method for monitoring corrosive impurities in molten $MgCl_2$/KCl/NaCl salts for thermal energy storage. In: Proceedings of 11th International Renewable Energy Storage Conference (IRES 2017), Düsseldorf Germany, 2017, Paper-Nr: IRES2017-141
26. Gaune-Escard M, ed. Molten Salts: From Fundamentals To Applications. NATO Science Series (Series II: Mathematics, Physics, and Chemistry), volume 52. Dordrecht: Springer, 2002, 283–285
27. Mohamedi M, Borresen B, Haarberg G M, Tunold R. Anodic

behavior of carbon electrodes in CaO-$CaCl_2$ melts at 1123 K. Journal of the Electrochemical Society, 1999, 146(4): 1472–1477

28. Brookes H C. Voltammetric investigations of $CaCI_2$:KCI melts at 700 °C. Journal of the Electrochemical Society, 1988, 135(2): 373–377
29. Liu B, Wei X, Wang W, Lu J, Ding J. Corrosion behavior of Ni-based alloys in molten NaCl-$CaCl_2$-$MgCl_2$ eutectic salt for concentrating solar power. Solar Energy Materials and Solar Cells, 2017, 170: 77–86
30. Vignarooban K, Pugazhendhi P, Tucker C, Gervasio D, Kannan A M. Corrosion resistance of Hastelloys in molten metal-chloride heat-transfer fluids for concentrating solar power applications. Solar Energy, 2014, 103: 62–69
31. Vignarooban K, Xu X, Wang K, Molina E E, Li P, Gervasio D, Kannan A M. Vapor pressure and corrosivity of ternary metal-chloride molten-salt based heat transfer fluids for use in concentrating solar power systems. Applied Energy, 2015, 159: 206–213
32. Gomez-Vidal J C, Tirawat R. Corrosion of alloys in a chloride molten salt (NaCl-LiCl) for solar thermal technologies. Solar Energy Materials and Solar Cells, 2016, 157: 234–244
33. Wang J W, Zhang C Z, Li Z H, Zhou H X, He J X, Yu J C. Corrosion behavior of nickel-based superalloys in thermal storage medium of molten eutectic NaCl-$MgCl_2$ in atmosphere. Solar Energy Materials and Solar Cells, 2017, 164: 146–155
34. Abramov A V, Polovov I B, Volkvich V A, Rebrin O I, Denisov E I, Griffiths T R. Corrosion of austenitic steels and their components in vanadium-containing chloride melts. ECS Transactions, 2012, 50 (11): 685–698
35. Gaune-Escard M, Haarberg G M, eds. Molten Salts Chemistry and Technology. Chichester: John Wiley & Sons, Ltd., 2014, 427–448
36. Gomez-Vidal J C, Fernandez A G, Tirawat R, Turchi C, Huddleston W. Corrosion resistance of alumina-forming alloys against molten chlorides for energy production. II: Pre-oxidation treatment and isothermal corrosion tests. Solar Energy Materials and Solar Cells, 2017, 166: 222–233
37. Wang J W, Zhou H X, Zhang C Z, Liu W N, Zhao B Y. Influence of $MgCl_2$ content on corrosion behavior of GH1140 in molten NaCl-$MgCl_2$ as thermal storage medium. Solar Energy Materials and Solar Cells, 2018, 179: 194–201
38. Hamer W J, Malmberg M S, Rubin B. Theoretical electromotive forces for cells containing a single solid or molten chloride electrolyte. Journal of the Electrochemical Society, 1956, 103(1): 8–16
39. Plambeck J A. Electromotive force series in molten salts. Journal of Chemical & Engineering Data, 1967, 12(1): 77–82
40. Indacochea J E, Smith J L, Litko K R, Karell E J, Rarez A G. High-temperature oxidation and corrosion of structural materials in molten chlorides. Oxidation of Metals, 2001, 55(1-2): 1–16
41. Indacochea J E, Smith J L, Litko K R, Karell E J. Corrosion performance of ferrous and refractory metals in molten salts under reducing conditions. Journal of Materials Research, 1999, 14(5): 1990–1995
42. Garcia-Diaz B L, Olson L, Martinez-Rodriguez M, Fuentes R, Colon-Mercado H, Gray J. High temperature electrochemical engineering and clean energy systems. Journal of the South Carolina Academy of Science, 2016, 14(1): 11–14
43. Gomez-Vidal J C, Fernandez A G, Tirawat R, Turchi C, Huddleston W. Corrosion resistance of alumina-forming alloys against molten chlorides for energy production. I: Pre-oxidation treatment and isothermal corrosion tests. Solar Energy Materials and Solar Cells, 2017, 166: 222–233
44. Gomez-Vidal J C. Corrosion resistance of MCrAlX coatings in a molten chloride for thermal storage in concentrating solar power applications. Nature Partner Journal Materials Degradation, 2017, 7: 1–9
45. Azarbayjani K, Rizvi G, Foroutan F. Evaluating effects of immersion tests in molten copper chloride salts on corrosion resistant coatings. International Journal of Hydrogen Energy, 2016, 41(19): 8394–8400